

Observation of the enhancement of electric fields normal to the surface using mid-infrared slot antennas and an atomic layer deposition technique

**Y. Nishimura¹, T. Kawano¹, Y. Kunichika¹, K. Kasahara^{1*}, T. Yaji¹,
N. Ikeda², H. Oosato², H. Miyazaki², Y. Sugimoto²**

¹ *Ritsumeikan University, 1-1-1 Noji-higashi, Kusatsu, Shiga 525-8577, Japan*

² *National Institute for Materials Science, 1-2-1 Sengen, Tsukuba, Ibaraki 305-0047, Japan*

E-mail address: kasaharat@se.ritsumei.ac.jp

Abstract

Optical electric field enhancement in the normal direction was experimentally investigated using mid-infrared slot antennas that were formed on a thin Al₂O₃ layer/Si substrate. The Al₂O₃ layer thicknesses could be controlled to an accuracy of a given atomic layer through the use of atomic layer deposition, and varied from 0 nm to 60 nm. An in-depth probe of the electric field was performed by observing the change in the reflection signal arising from the Restrahlen band of the natural oxide of Si formed on the surface of a Si substrate. In contrast to dipole nanoantennas, we could clearly observe Restrahlen bands of Al₂O₃ as well as the native Si oxide film. This was because the direction of the enhanced electric field was primarily parallel to the substrate surface in the slot antennas, which was different from the dipole nanoantenna having strong normal electric fields at the antenna ends. The atomic layer deposition technique provides versatile information on the electric field distribution within the depth direction, being considered complementary to the electromagnetic simulation of nanoantennas.

1. Introduction

Significant progress in mid-infrared distributed-feedback quantum cascade lasers (QCLs) capable of continuous-wave operation above room temperature has allowed for the monitoring of trace gases relating to environmental and energy issues [1], [2]. To broaden the application of QCLs, photo-detectors exhibiting both high-sensitivity and high-speed are needed in the mid-infrared range. Optical antennas generate optical hotspots, and enhance local field intensity near the antenna, thereby allowing for efficient photon harvesting [3]. Thus, sufficient absorption is obtainable even from a thin absorption layer, and it is possible that a combination of optical antennas and a thin photo-absorption layer [4-6] leads to the achievement of high-performance mid-infrared detectors with high-sensitivity and quick response times. Field intensity becomes large near an antenna, and decreases rapidly with increasing distance from it. Accordingly, it is necessary to know the increased field distribution of the antenna in the vertical direction for designing mid-infrared photo-detectors equipped with antennas. The finite-difference time-domain (FDTD) method is a powerful tool for use in the design of nano-optical devices, which can calculate electric fields in the depth direction. However, it is still necessary to evaluate the appropriateness of the obtained results in a practical manner, because FDTD simulation necessitates the frequency dispersive nature of media in an analytical domain and very fine discretization in space in order to correctly predict the electromagnetic distribution, particularly, in the case of optical nanoantennas including metals. The field enhancement of the antenna can be measured by observing a reflection or transmission spectra through a micro-Fourier transform infrared (FT-IR) spectrometer [7-13]. Local information on the field enhancement is also available if one uses a scattering near-field microscopy (s-SNOM) [14]. However, such measurements alone are insufficient to ascertain the distribution of field enhancement normal to an antenna plane. To this end, a thin Al_2O_3 layer was deposited on a Si substrate through atomic layer deposition (ALD), and dumbbell-shaped slot antennas (DSAs) were fabricated on this. It was possible to grow a layer with thickness being controlled to an accuracy of ~ 1 nm. By observing the spectral magnitude dependence of the SiO_2 layer, which was naturally formed on the Si layer, on the Al_2O_3 thickness, we could actually gain an understanding of the vertical field localization. Unlike the surface-phonon polariton (SPhP) signals obtained in experiments using dipole nanoantennas, reflectivity increases originating from the Restrahlen band (or forbidden polariton band) of natural Si oxide film emerged, and we could measure their depth dependence. There have been no experiments reporting the distribution of electric field enhancement in the perpendicular direction. Reflectivity increases in the Restrahlen band due to the antenna effect were distinctly observed from ALD-made Al_2O_3 layers as well as from a SiO_2 layer. This was because the direction of the enhanced electric field was mainly parallel to the substrate surface in DSAs.

2. Fabrication of dumbbell-shaped slot antennas

The performances of optical antennas have been, so far, reported mainly using dipole structures. In this study, we used a DSA, which consisted of a rectangular opening with a small feed-gap in its center, which was cutout from a thin metal sheet [Fig. 1 (a)-(c)]. L and W represent the length and width of the rectangular opening, respectively, in the figure. The length and width of the feed-gap are denoted by A and G , respectively. The feed-gap formed a nano capacitor, leading to an intense localization of the electric field. In the radio-frequency range, the radiation pattern of a rectangular-shaped slot antenna is the same as that of a dipole antenna, with the sole difference being the reversed direction of the electric and magnetic fields. The optical dipole antenna has two hotspots at both ends. On the other hand, the DSA used in our study could easily form a single hotspot in the center [15], meaning that the DSA could convert an incident electromagnetic wave into a more localized volume, yielding increased absorption in a thinner layer. Another merit of the slot antenna is that its fabrication is easier than that of dipole antennas, because dipole antennas leave small metal stripes on substrates.

The slot antenna arrays were fabricated as follows: a thin Al_2O_3 was grown using ALD on a Si substrate. A set of cleaning processes including HF treatment is ordinarily performed to remove the Si oxide film naturally formed on a Si substrate prior to dielectric layer deposition, but this process was omitted to use the native oxide layer as a marker for investigating electric field distribution in the depth direction. ALD is a process for the deposition of highly uniform thin layers by alternating exposure of a surface to vapors from two chemical reactants in a viscous-flow reactor. Al_2O_3 -ALD was performed using trimethylaluminum (TMA) and H_2O along with commercially-available equipment. The non-uniformity of the nominal thickness was 0.3% in a 3-inch wafer. TEM images showed that Al_2O_3 ALD films grown at 200° C were smooth [Fig. 1 (d)]. Next, Au (40 nm)/Ti (10 nm) were deposited on the substrate. The thickness of Au was determined to be thicker than the skin depth of Au (26 nm). The plasmonic mode excited on the top surface of Au wasn't influenced by the bottom surface under these conditions, and the resonant frequency was not influenced by the thickness of the Au. Antenna patterns were made by electron-beam lithography and a lift-off technique followed, cutting out dumbbell-shaped openings from a metal sheet. The slot antenna in the radio-frequency domain resonates when the long side of a rectangle is half of the wavelength λ of the incident radiation. The scaling, however, fails in the mid-infrared range, since the metals act as a strongly-coupled plasma, and the length of the long side shortens. One antenna array consisted of 15 x 5 elements, each having the same size. Besides the antenna arrays, 30 $\mu\text{m} \times 30 \mu\text{m}$ square openings were formed to examine the antenna effect.

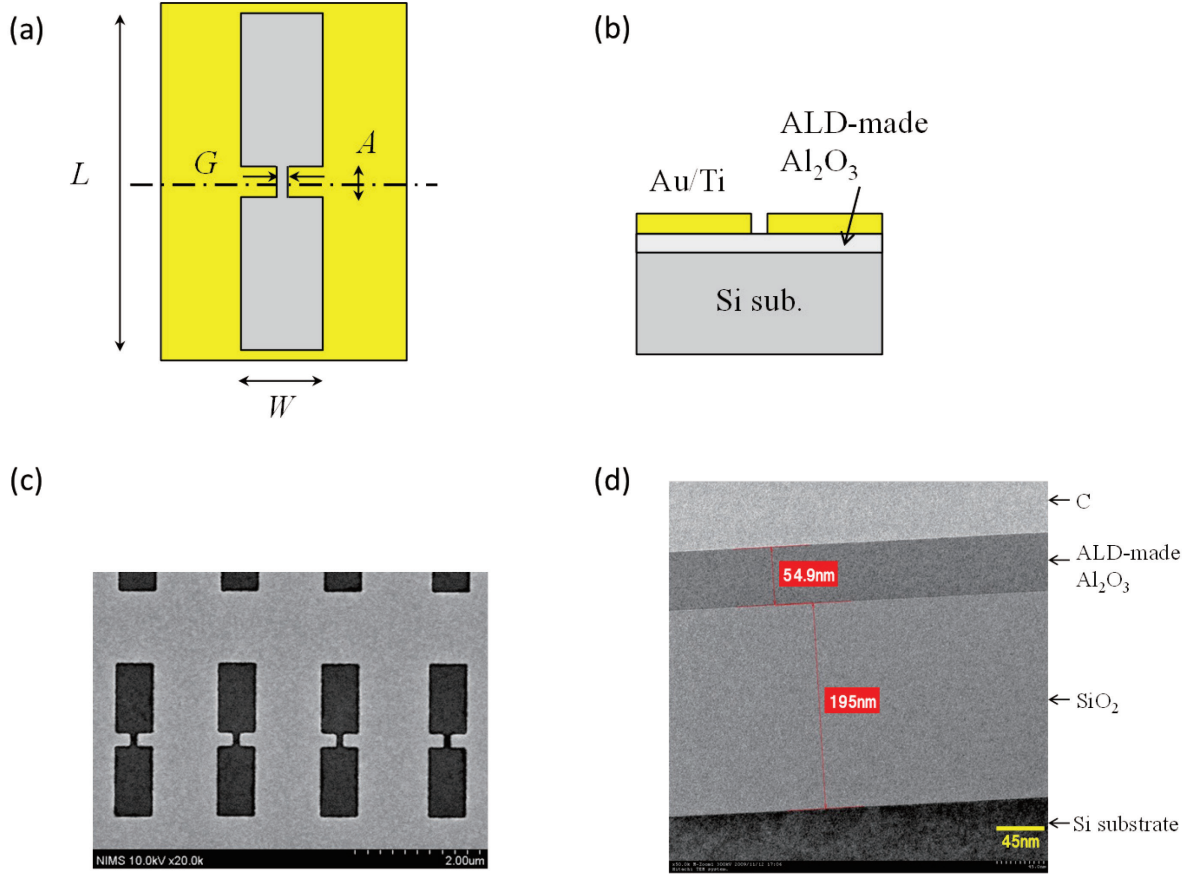
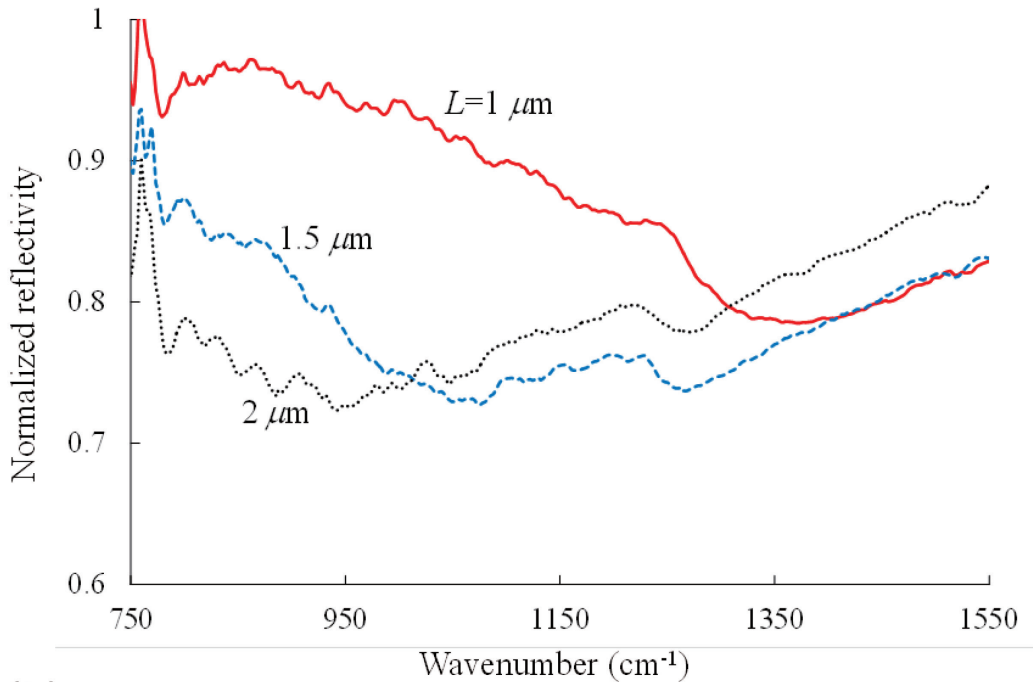


Fig. 1 Dumbbell-shaped antenna structure. (a) Plane view and (b) cross-sectional view. L : length, and W : width of the rectangular opening. A : length, and G : width of the feed-gap. (c) Surface image of the fabricated DSAs. (d) Cross-sectional view of a structure fabricated to measure the thickness of ALD-made Al_2O_3 using TEM. In this case, Al_2O_3 thickness is 54.9 nm.

3. Reflection spectra of antennas on the Si substrate

The reflection spectra were obtained using a microscopic FT-IR with a LN_2 -cooled mercury cadmium telluride detector. An incident wave with a 15-degree angle of obliquity was polarized with a metal grid polarizer. The reflection spectrum was normalized by the reflectivity of the Au film on the substrate. Normalized reflectivities of three arrays made on Si substrates are shown in Fig. 2 (a). The long side lengths of the individual antenna elements in the three arrays were 1, 1.5, and 2 μm . The polarization of incident light was directed parallel to the short sides of DSAs as resonance took place. The reflectivities corresponding to these arrays obtained from measurements in the non-resonant direction are also shown in Fig. 2 (b). The spectra in the resonant direction were distinctly different from those in the non-resonant direction.

(a)



(b)

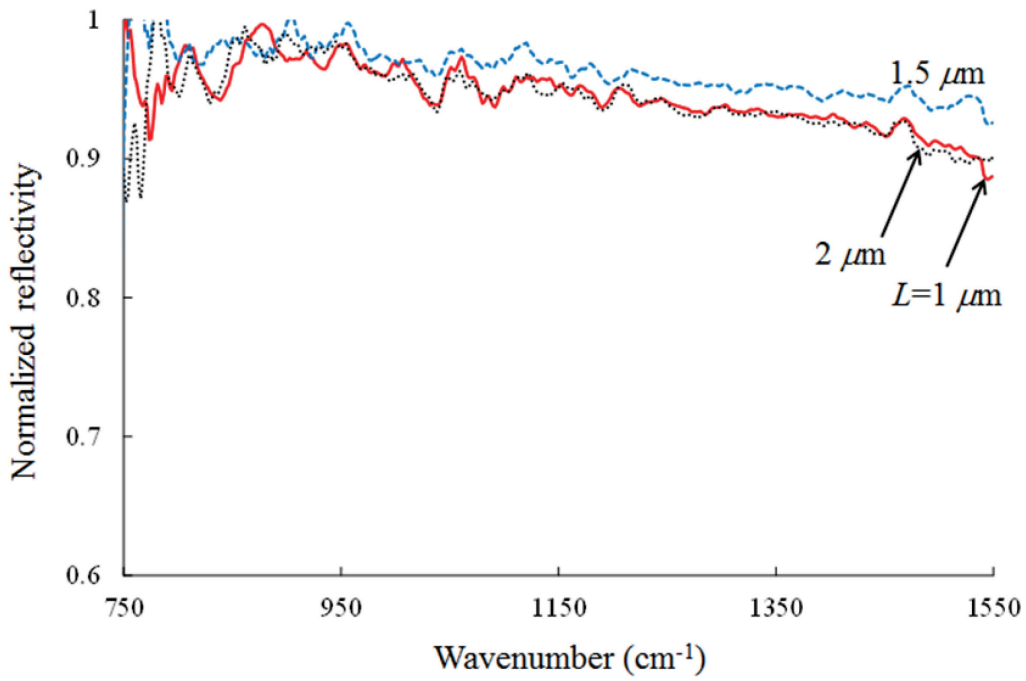


Fig. 2 Normalized reflectivity (a) in the resonant direction, and (b) in the non-resonant direction for $L = 1, 1.5$, and $2\text{ }\mu\text{m}$. $W = 0.6\text{ }\mu\text{m}$, $A = 0.4\text{ }\mu\text{m}$, and $G = 0.1\text{ }\mu\text{m}$. Each array consists of 15×5 dumbbell-shaped elements.

One finds that the reflectivities in Fig. 2 (a) show characteristic features around 1050~1250 cm⁻¹ which were different from resonant properties. The resonant wavelength of the array with the long side length, $L = 1 \mu\text{m}$ was around 1350 cm⁻¹, and the change between 1050 cm⁻¹ and 1250 cm⁻¹ was not necessarily clear in the figure. However, reflectivity increases were clearly seen for $L = 1.5$ and $2 \mu\text{m}$ arrays. Such increases didn't appear for an area without antenna elements, which primarily reflected the optical absorption property of bulk Si. Field enhancement occurred in the vicinity of antennas, and it was reasonably concluded that the reflectivity increases were caused by a thin SiO₂ layer which had been formed naturally on the Si substrate. A signal stemming from the SPhP of the natural oxide of a Si wafer was observed below the longitudinal optical (LO) phonon frequency, ω_L at 1251 cm⁻¹, of SiO₂ in FTIR transmission measurements using gold nanowires [12], [13]. Our results were obviously different from the signal arising from SPhP. Judging from the transverse optical (TO) frequency, ω_T at 1065 cm⁻¹ and the LO frequency of SiO₂, the region where the reflectivity grew corresponded to the Restrahlen band of SiO₂ in which there was no bulk polariton to transmit radiation, and all incident power was reflected at the interval $\omega_T < \omega < \omega_L$. This region was unobservable without antenna elements because the incident electro-magnetic wave was weak. Forming an antenna array on a Si substrate concentrated the electric field on spots near the Si surface, leading to the resultant appearance of the distinguishing reflection.

In order to confirm the above results, we prepared samples consisting of SiO₂ on Si substrates without DSAs, and measured their reflection spectra (Fig. 3). SiO₂ was deposited on a Si substrate using thermal chemical vapor deposition. The thicknesses of SiO₂ were 50, 100, and 200 nm. A similar increase in the reflectivity between 1050 and 1250 cm⁻¹ started to be observed, which did not contradict the above supposition. So far, it has been reported that SPhP-originated signals could be detected using gold nanoantennas formed on Si substrates. The nanoantenna could generate an intense normal electric field at both of its ends, making the observation of SPhP signals possible. In the case of DSAs, however, primary electric fields are parallel to the substrate, and they were enhanced by the antenna, particularly at the center portion with being narrow in width. Therefore, ordinary absorption seen in bulk should be observed, but to the authors' knowledge, there were little experimental data which clearly showed the appearance of the Restrahlen reflection of a dielectric layer as thin as a few nm owing to the optical antenna effect [13].

The length of the central part of an antenna, A , had a profound effect on the resonant wavelength as well as on L , compared with W and G , associated with the short side length. When A was lengthened while L was fixed, the resonant wavenumber shifted to longer wavelengths (Fig. 4).

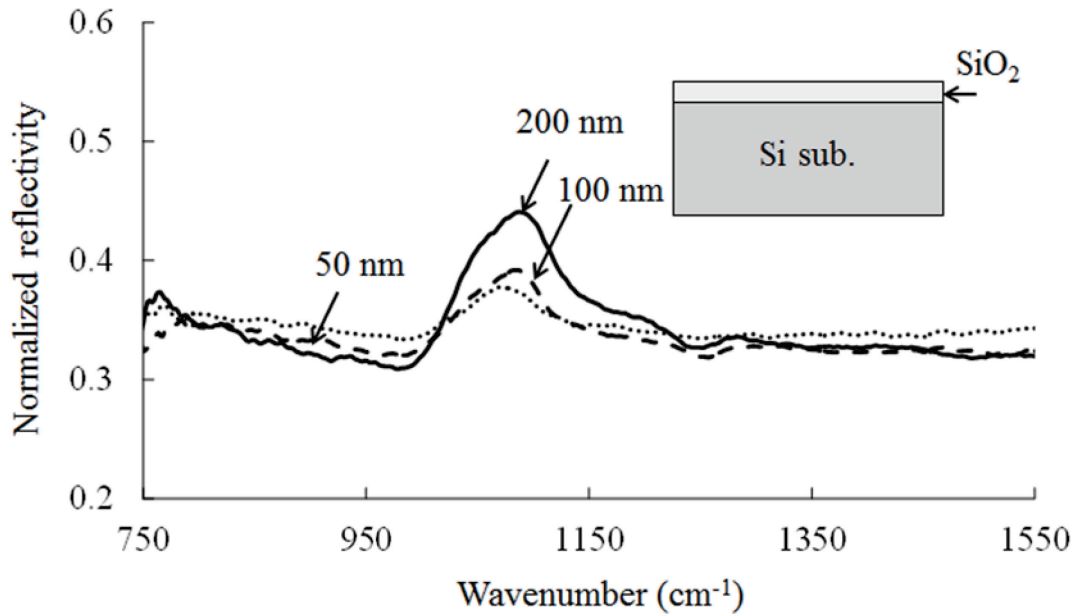


Fig. 3 Normalized reflectivity of SiO₂ on Si substrate without DSAs. The thicknesses of SiO₂ are 50, 100, and 200 nm.

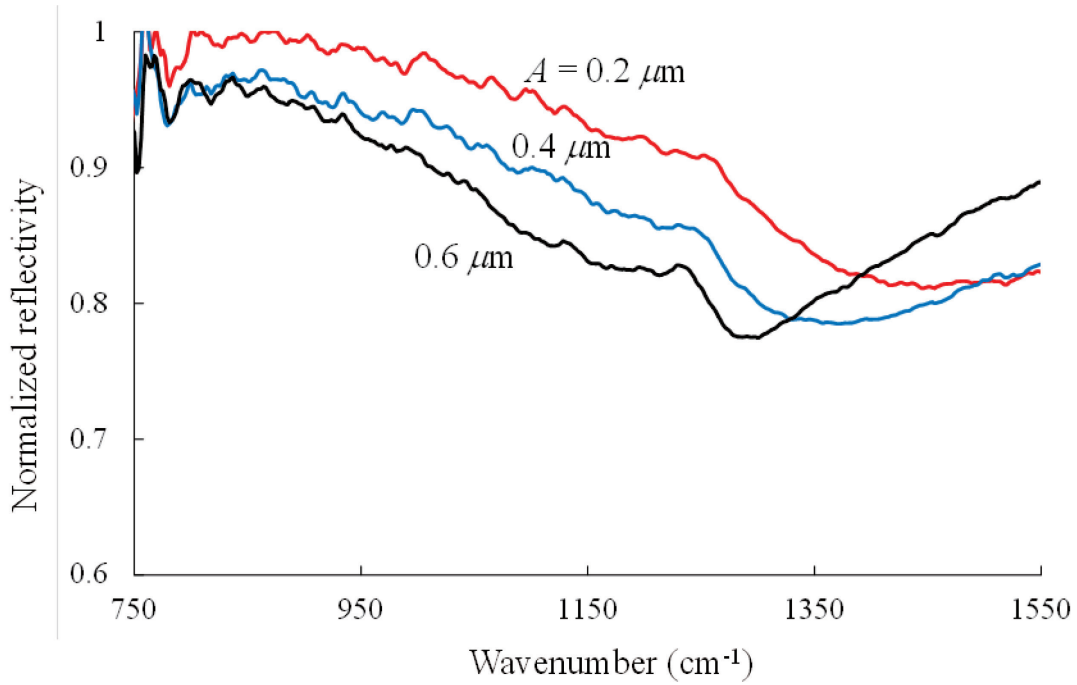


Fig. 4 Normalized reflectivity for $A = 0.2, 0.4$, and $0.6 \mu\text{m}$. $L = 1 \mu\text{m}$, $W = 0.6 \mu\text{m}$, and $G = 0.1 \mu\text{m}$.

4. Reflection spectra of antennas on $\text{Al}_2\text{O}_3/\text{Si}$ substrates

The results for antenna arrays on $\text{Al}_2\text{O}_3/\text{Si}$ substrates are shown in Fig. 5. The thicknesses of the ALD-made Al_2O_3 were 0, 20, 40, and 60 nm. Depositing Al_2O_3 on a Si substrate caused major changes in the spectrum. The reflectivity-increase region corresponding to the Restrahlen band of SiO_2 weakened as the Al_2O_3 was deposited and thickness increased. Characteristic features almost disappeared for the 60-nm Al_2O_3 , meaning that the electric field in a natural SiO_2 layer weakened with increases in the thickness of Al_2O_3 . Instead, it was observed that the reflectivity became high in the frequency range centered around 850 cm^{-1} when an Al_2O_3 layer was inserted. The reflectivity in the region became high when inserting a 20-nm Al_2O_3 layer, and the changes in that region were small for 40 and 60 nm. Such reflectivity increases were never observed in the measurements for the 60-nm $\text{Al}_2\text{O}_3/\text{Si}$ without antennas: the reflection spectrum was almost completely identical to that of Si because the Al_2O_3 layer was very thin. Judging from this, it is concluded that the observed reflection increase of around 850 cm^{-1} was due to the Restrahlen reflection of Al_2O_3 through the electric-field enhancing effects of DSAs. The imaginary part of the refractive index of $\alpha\text{-Al}_2\text{O}_3$ (sapphire) reaches its maximum at 580 cm^{-1} [16-18]. Thus, the observed Restrahlen band appeared to have been situated at higher frequencies, which will be discussed in the following section.

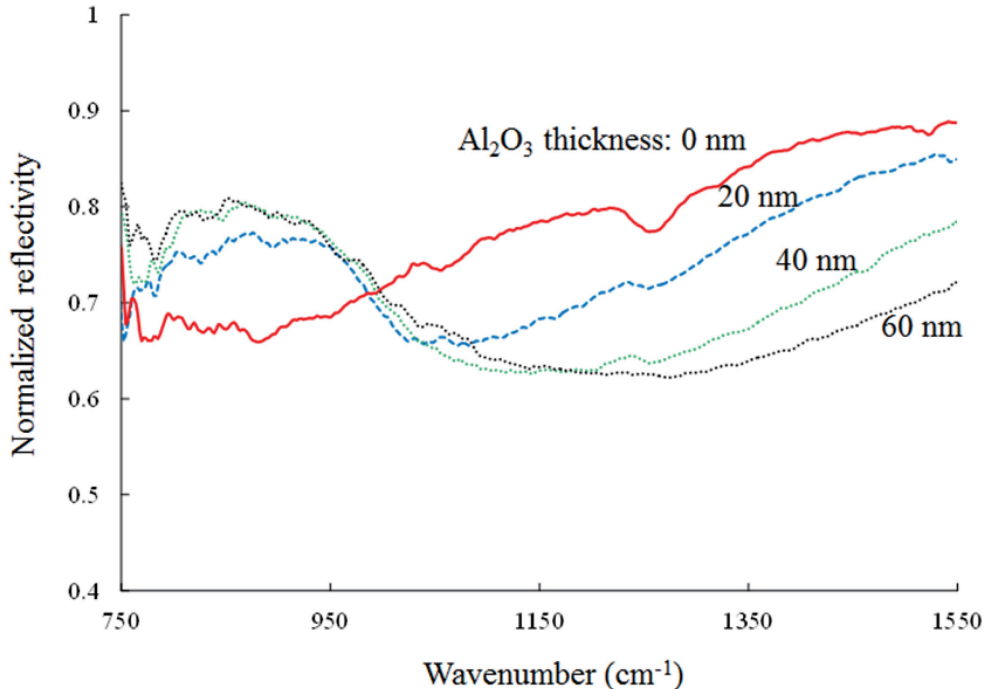


Fig. 5 Normalized reflectivity from a DSA array formed on an $\text{Al}_2\text{O}_3/\text{Si}$ substrate. Each element of the array: $L = 2.5 \mu\text{m}$, $W = 0.6 \mu\text{m}$, $A = 0.6 \mu\text{m}$, and $G = 0.1 \mu\text{m}$. The thicknesses of Al_2O_3 are 0, 20, 40, and 60 nm.

5. Discussions

We have successfully observed the Reststrahl band of SiO_2 formed naturally on Si through the effect of the electric field amplification of DSAs. Its thickness should be within the order of nanometers. So, one might think about the necessary thickness for such a reflection window to be observed without optical antennas, and might think that about half of the wavelength of the radiation concerned is required as the thickness of the surface zone. However, the question of what will become of the Reststrahl reflection if the thickness is less than the wavelength has not necessarily been answered. According to the results shown in Fig. 3, one finds that the characteristic spectra can be seen even with the SiO_2 thickness as thin as 50 nm which is two-hundredth the incident wavelength in a vacuum. The signal was, of course, weaker with decreasing SiO_2 thickness, and it was certain that a few-nm thin SiO_2 layer could not be detected without optical antennas.

To understand the observation data obtained from the reflection spectra on $\text{Al}_2\text{O}_3/\text{Si}$ with DSAs, and to examine to what extent the measurement data were coincident with the results of the electromagnetic analysis, we performed FDTD simulations. Figure 6 shows calculated results with the corresponding measurements. Non-uniform mesh was used in the simulation, and the minimum mesh size was 0.5 nm in the vertical direction. Perfectly matched layer conditions were used for the top and bottom boundaries, and periodical boundary conditions were employed for others. We assumed that the thickness of natural Si oxide film was 2 nm. For the refractive index of Al_2O_3 , we used the data determined by using an ellipsometer, because we found that the use of an $\alpha\text{-Al}_2\text{O}_3$ refractive index couldn't explain the experimental results: the calculated Restrahlen band of Al_2O_3 turned out to appear at frequencies lower than those in reality. ALD-made Al_2O_3 layers grown at such temperatures as low as 200° C were amorphous. Accordingly, the refractive index data of the ALD-made Al_2O_3 was taken with an ellipsometer, and they were used in the simulation. The center frequency of the reflectivity bump became 850 cm^{-1} and was in good agreement with the measurements, including the saturation characteristics of increasing Al_2O_3 thickness. The calculated spectra coincided approximately with the experimental results except that overall, the calculated reflectivity was higher than in the measured result. This was probably because we used the values listed in ref. [16] as the refractive index of the Si substrate, which were the data of non-doped Si, and the actual substrate was n-doped. Another possible reason behind the difference was accuracy limitations of FDTD: it was difficult to accurately obtain the enhancements at the metal/dielectric interfaces because of memory limitations.

Figure 7 (a) and (b) show the wavelength dependence of the enhancement of E_x^2 (E_x : electric field parallel to the substrate surface) at $x = 40 \text{ nm}$ (near the edge of Au) and 0 nm (center of the gap), respectively. Calculations were performed for a structure consisting of a DSA attached on Si. Antenna size was the same as that used in the experiments shown in Fig. 5. Depth was defined given the distance from the Si surface at $z = 0 \text{ nm}$ (the z-axis is taken

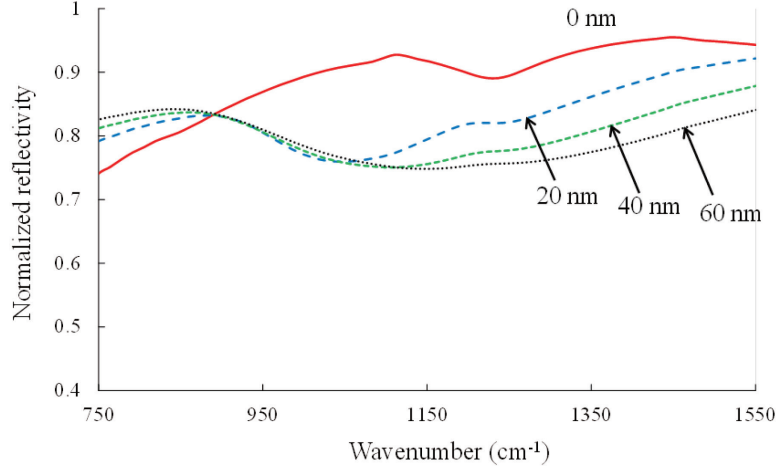


Fig. 6 FDTD simulation results corresponding to the experimental results shown in Fig. 5. The thickness of SiO_2 is assumed to be 2 nm.

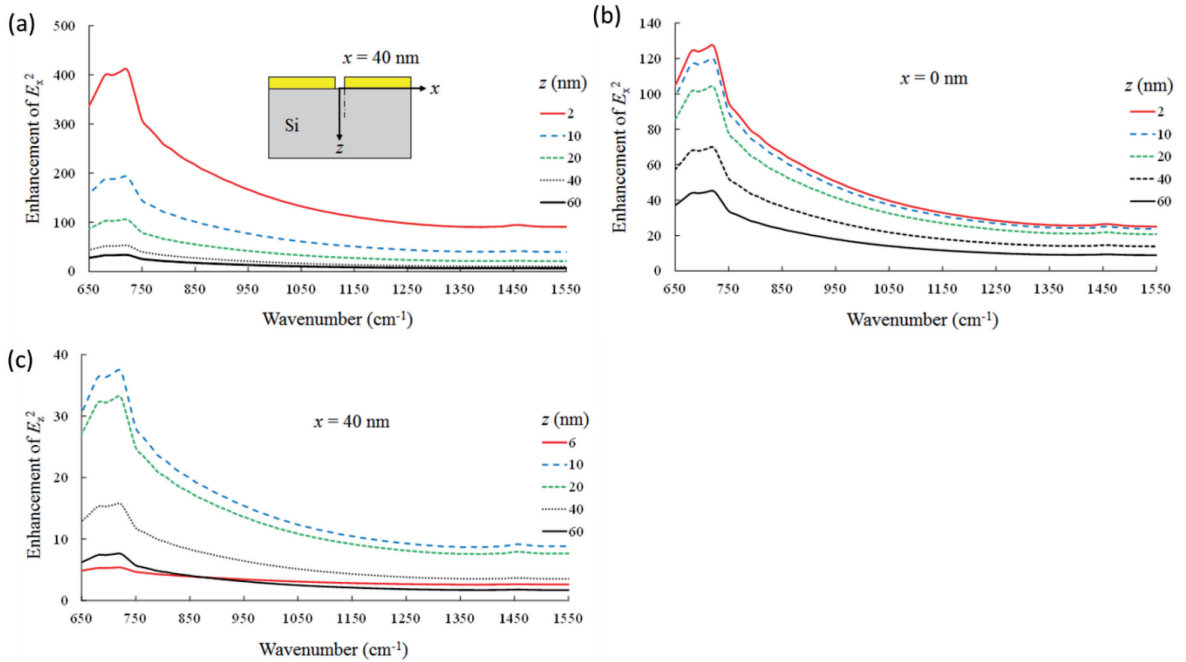


Fig. 7 Enhancement of (a) E_x^2 at $x = 40 \text{ nm}$, (b) E_x^2 at $x = 0 \text{ nm}$, and (c) E_z^2 at $x = 40 \text{ nm}$ vs. wavenumber for a DSA array on Si. Depth is taken as a parameter. The L , W , A , and G of each element of the array are the same as the parameters used in the experiments shown in Fig. 5.

toward the Si substrate). E_z^2 (E_z : electric field normal to the substrate) at $x = 40$ nm is shown in Fig. 7 (c). The incident electric field, E_{x0} , was directed toward the resonant direction of the DSA, and E_x^2 and E_z^2 were normalized by E_{x0}^2 in the figures. At a position of $z = 2$ nm, the maximum enhancement of E_x^2 at $x = 40$ nm was 400 at the resonance wavelength of 725 cm^{-1} ($13.8 \mu\text{m}$), and it was 100 at 1250 cm^{-1} where the LO phonon of SiO_2 appeared. On the other hand, at $x = 0$ nm, they were 120 and 30, respectively. For E_z^2 at $x = 40$ nm, the maximum enhancement occurred at $z = 10$ nm. Comparing E_z^2 with E_x^2 at $x = 40$ nm, maximum enhancement of E_z^2 was about one tenth of E_x^2 . E_z^2 was zero at $x = 0$ nm. This accounts for why SPhP wasn't observed and that only the Restrahlen reflection appeared. Figure 8 shows the enhancements of E_x^2 and E_z^2 for a DSA on 2-nm SiO_2/Si . In comparison with the case without 2-nm SiO_2 , the maximum E_x^2 enhancement at 725 cm^{-1} ($x = 40$ nm and $z = 2$ nm) decreased from 400 to 300. In the range between 1110 cm^{-1} and 1220 cm^{-1} which was almost equivalent to the Restrahlen band of SiO_2 , E_x^2 decreased sharply. This is because reflection occurs and the internal electric field weakens in this interval.

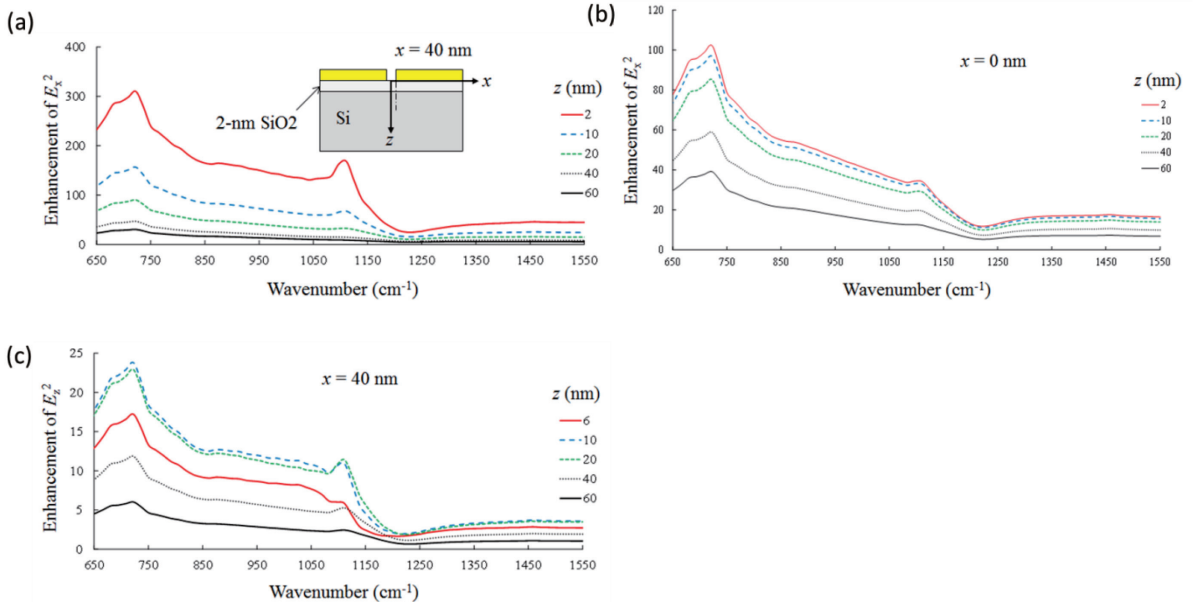


Fig. 8 Enhancement of (a) E_x^2 at $x = 40$ nm, (b) E_x^2 at $x = 0$ nm, and (c) E_z^2 at $x = 40$ nm vs. wavenumber for a DSA array on 2-nm SiO_2/Si .

The enhancements of E_x^2 at the resonant frequency of 750 cm^{-1} with a DSA on Si are shown as a function of depth (or z) in Fig. 9 (a). They were calculated at $x = 40, 20$, and 0 nm . E_x^2 at $x = 40 \text{ nm}$ decreased rapidly as the position was distant from the Si surface, and was half at $z = 8 \text{ nm}$. At $z = 20 \text{ nm}$, the enhancement became almost the same as those at $x = 0 \text{ nm}$ and 20 nm . Then, E_x^2 attenuated nearly linearly with z . The decay behavior of E_x^2 at 1250 cm^{-1} almost scaled that at the resonant wavelength [Fig. 9 (b)]. Figures 10 (a) and (b) show the enhancements of E_z^2 at 725 cm^{-1} and 1250 cm^{-1} , respectively. While E_x^2 decreased as the position moves further away from the Si surface, E_z^2 at $x = 40 \text{ nm}$ showed a maximum at $z = 12 \text{ nm}$. This is easily anticipated from the following: although E_z is zero on the surface of the substrate, it starts to appear with distance from the surface. E_z eventually vanishes at a great distance, thereby leading to the existence of a peak. E_z^2 disappears at the center of the gap ($x = 0 \text{ nm}$).

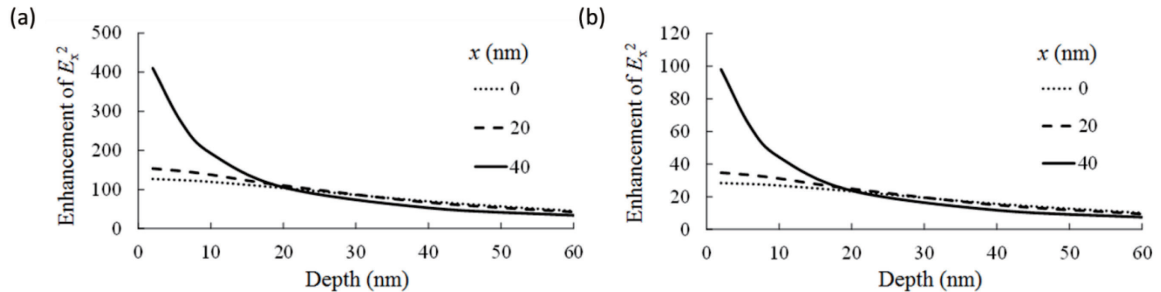


Fig. 9 Enhancements of (a) E_x^2 at the resonant wavelength of 750 cm^{-1} , and (b) non-resonant 1250 cm^{-1} vs. depth for a DSA array on Si. $x = 40, 20$, and 0 nm . The L, W, A , and G of each element of the array are the same as the parameters shown in Fig. 5.

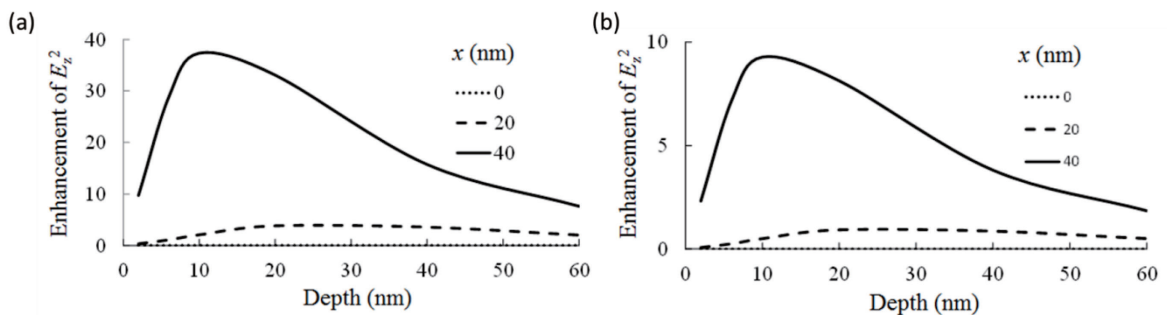


Fig. 10 Enhancements of E_z^2 vs. depth corresponding to Fig. 9 for (a) 750 cm^{-1} , and (b) 1250 cm^{-1} .

In increasing the thickness of Al_2O_3 on Si, the Restrahlen signal attenuated and faded out when the thickness reached 60 nm. According to the results shown in Fig. 3 indicating the dependence of the Restrahlen reflectance on SiO_2 thickness, it is not strange that the Restrahlen signals appeared for ~ 2 -nm thick SiO_2 through the enhancement of E_x^2 . In our micro FT-IR experiments, transmission was negligibly small because of the use of n-doped Si substrate. This means that reflectivity = (1-absorptivity). Absorptivity of the ALD-made $\text{Al}_2\text{O}_3/\text{natural Si oxide/Si}$ in which optical antennas aren't attached to the surface equals $I_0(\alpha_1 \Delta z_1 + \alpha_2 \Delta z_2 + \alpha_3 \Delta z_3)$, where I_0 : incident light, α : absorption coefficient, Δz : layer thickness, and subscripts of 1, 2, and 3 denote Al_2O_3 , SiO_2 , and Si, respectively. Antennas were effective in enhancing I_0 by increasing E_x^2 , thereby resulting in equivalently increasing Δz . On the surface of Si with a DSA, the enhancement of E_x^2 for 1250 cm^{-1} at $z = 2 \text{ nm}$ was 100 at $x = 40 \text{ nm}$ and was 30 at $x = 0 \text{ nm}$ [Figs. 7 (a) and (b)]. This means that the equivalent SiO_2 layer thickness reached 30~100 times the actual thickness (i.e. assuming that the natural oxide layer was 2 nm, it was 60 nm~200 nm). The Restrahlen signal was observed with 50-nm SiO_2 even under antennaless conditions. Therefore, it is no wonder that the signal emerged from a Si wafer which was covered by a thin layer of natural oxide through DSAs. According to the results shown in Figs. 9 (a) and (b), the enhancement of E_x^2 at $z = 60 \text{ nm}$ becomes 8% of that at $z = 2 \text{ nm}$, which was consistent with the experimental results shown in Fig. 5.

Light elastically scattered from an object located near the antenna might offer a possibility of increasing the reflectivity further. Surface-enhanced light scattering was reported to occur through the use of an optical antenna, and the intensity elastically scattered off an object that was near the optical antenna was proportional to the fourth power of the local field enhancement provided by the antenna. The underlying electromagnetic mechanism of this phenomenon was also noted as being the same as the one generally acknowledged to be at work in surface-enhanced Raman scattering [19]. Thus, we examined whether the reflectance spectra were subject to the influence of incident radiation. If the scattering had an effect on the spectra, the spectra should have made a difference by changing the input light power of the FT-IR. However, no change was observed in the spectra, and the influence of scattering on the measured results was negligible in our experiments.

6. Conclusion

The vertical distribution of the electric field produced by optical antennas could be experimentally confirmed through the utilization of the ALD technique. Experimental results were compared with FDTD calculation. Measured results were in reasonable quantitative agreement with the FDTD calculation, but strictly speaking, it was found that there were some points which were unaccountable for from the simulation, which wasn't universal in predicting the electromagnetic distribution in optical devices, particularly with nanoantennas.

Combing the FDTD method with the ALD technique allows for more accurate analysis of field enhancements in the perpendicular direction. Furthermore, one could also obtain accurate spatial electric field information in the use of s-SNOM in conjunction with the ALD.

Acknowledgements

We would like to thank M. Ochiai for device fabrication. This work was supported by JSPS KAKENHI Grant Number 23560043, and Nano-Integration Foundry (NIMS) in "Nanotechnology Platform Project" operated by the Ministry of Education, Culture, Sports, Science and Technology (MEXT), Japan.

References

- [1] Wysocki, G. et al., *Appl. Phys. B* **92**, 305-311 (2008).
- [2] Kumazaki, N. et al., *Appl. Phys. Lett.* **92**, 121104 (2008).
- [3] Crozier, K.B. et al., *J. Appl. Phys.* **94**, 4632-4642 (2003).
- [4] Wu, W. et al., *Appl. Phys. Lett.* **96**, 161107 (2010).
- [5] Knight, M.W. et al., *Science* **332**, 702-704 (2011).
- [6] Horikawa, J. et al., 2013 Conference on Lasers and Electro-Optics Pacific Rim (CLEO-PR), WPC-10 (2013).
- [7] Enders, D. et al., *Appl. Phys. Lett.* **88**, 184104 (2006).
- [8] Olmon, R.L. et al., *Opt. Express* **16**, 20295-20305 (2008).
- [9] Neubrech, F. et al., *Phys. Rev. Lett.* **101**, 157403 (2008).
- [10] Adato, R. et al., *PNAS* **106**, 19227-19232 (2009).
- [11] Jones, A.C. et al., *Nano Lett.* **9**, 2553-2558 (2009).
- [12] Neubrech, F. et al., *J. Phys. Chem. C* **114**, 7299-7301 (2010).
- [13] Neubrech, F. et al., *IEEE J. Select. Topics Quantum Electron.* **19**, 4600809 (2013).
- [14] Schnell, M. et al., *Nano Lett.* **10**, 3524-3528 (2010).
- [15] Kumar, V.D. et al., *Photon. and Nanostruct.* **7**, 161-168 (2009).
- [16] Palik, E.D., *Handbook of optical constants of solids, second ed.*, Academic Press, San Diego (1985).
- [17] Schubert, M. et al., *Phys. Rev. B* **61**, 8187-8201 (2000).
- [18] Bozec, D. et al., *J. Appl. Phys.* **91**, 8795-8797 (2002).
- [19] Alonso-Gonzalez, P. et al., *Nat. Commun.* **3**, 684 (2012).